



Measurement of effective $^{98}\text{Mo}(n,\gamma)^{99}\text{Mo}$ reaction cross-section in the epi-cadmium neutron flux produced by 10 MeV electron LINAC with Ta-BeO assembly

Kapil Deo¹ · Rajeev Kumar^{1,2} · Amod K. Mallick¹ · Sudipta Samanta¹ · Deep Bhandari¹ · Anindita Sarkar¹ · K. Umasankari^{1,2} · Nishant Chaudhary^{3,2} · Amar D. Pant⁴ · Amit Verma⁴ · P. Anilkumar⁴

Received: 1 November 2023 / Accepted: 20 April 2024
© The Author(s) 2024

Abstract

An experiment was carried out to study the feasibility of ^{99}Mo production using an electron accelerator based epi-cadmium neutron source. The neutrons were produced by the interaction of bremsstrahlung end-point energy of 10 MeV with BeO blocks and the neutrons thus produced were moderated using High Density Polyethylene blocks. Effective cross-section of $^{98}\text{Mo}(n,\gamma)^{99}\text{Mo}$ reaction was measured using foil activation method. An enhancement in the effective cross-section due to resonances in the epi-cadmium region was observed. The photons and neutron production/transport in the experimental set-up were simulated using the FLUKA Monte Carlo code. The simulations were found to be in good agreement with the experimental findings.

Keywords $^{98}\text{Mo}(n,\gamma)^{99}\text{Mo}$ reaction · $^{99}\text{Mo}/^{99\text{m}}\text{Tc}$ Medical radioisotopes · Electron accelerator · Epi-cadmium neutrons · Ta-BeO assembly

Introduction

Technetium-99 m Radiopharmaceuticals are the major diagnostic tool in the clinical practice of nuclear medicine worldwide. $^{99\text{m}}\text{Tc}$ is the daughter product of ^{99}Mo . The latter has a half-life of 65.94 h. Almost all supply of ^{99}Mo (nearly 90%) required for $^{99\text{m}}\text{Tc}$ generators is produced by the neutron-induced fission of ^{235}U targets in nuclear research reactors [1]. A relatively lesser amount (~ 10%) is produced by low energy neutron capture in ^{98}Mo . In recent years, the ^{99}Mo supply crisis occurred as a result of various factors such as the extension of planned outages and the prolonged or

unplanned shutdown of many reactors around the world [1–3]. With the aim of mitigating these supply-side disruptions, alternative routes for production of ^{99}Mo are being explored. These include photo-neutron reaction [$^{100}\text{Mo}(\gamma, n)^{99}\text{Mo}$] [4, 5], photo-fission reaction [$^{238}\text{U}(\gamma, f)$] using high energy electron accelerators [6, 7], and fast neutron induced reactions [$^{100}\text{Mo}(n, 2n)$] [8–10]. Production of radioisotopes using particle accelerators has the advantages of negligible nuclear wastes in comparison to nuclear reactors, relatively lower cost, and higher availability. In view of higher availability and economical operation, electron accelerators are an attractive choice for the production of radioisotopes.

In the present work, an exploratory experiment was carried out to study the feasibility of ^{99}Mo production using (e- γ -n) cascade reaction. A high energy electron beam was made to fall on a high Z target (Ta). The bremsstrahlung photons thus produced were then made to strike BeO blocks. The photo-neutrons produced [11], were then utilised for neutron capture reaction in ^{98}Mo . Being a two-step process, the efficiency of this route is expected to be lower. However, the fast spectrum of neutrons produced can be shifted to the epi-cadmium energy region. Hence, there exists a possibility to increase the yield of ^{99}Mo . The reaction $^{98}\text{Mo}(n,\gamma)^{99}\text{Mo}$ has distinct resonances in the epi-cadmium region. Figure 1

✉ Rajeev Kumar
rajeevk@barc.gov.in

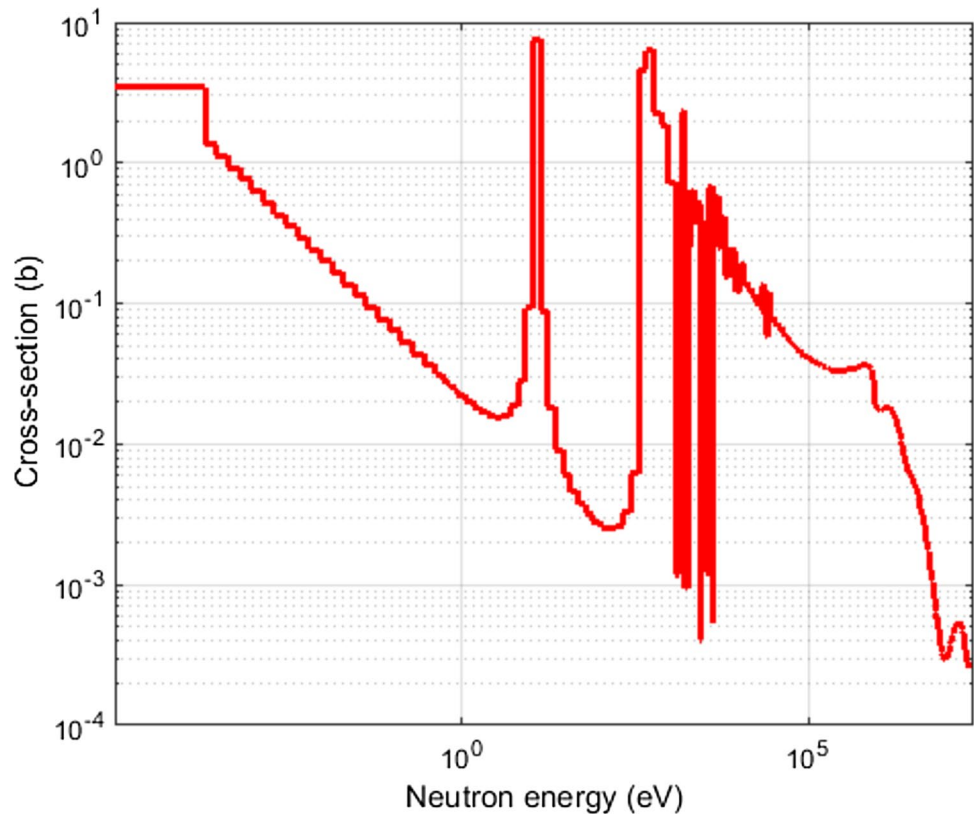
¹ Reactor Physics Design Division, Bhabha Atomic Research Center, Mumbai 400085, India

² Homi Bhabha National Institute, Bhabha Atomic Research Center, Mumbai 400085, India

³ Accelerator and Pulse Power Division, Bhabha Atomic Research Center, Mumbai 400085, India

⁴ Environmental Monitoring and Assessment Division, Bhabha Atomic Research Center, Mumbai 400085, India

Fig. 1 $^{98}\text{Mo}(n,\gamma)^{99}\text{Mo}$ reaction cross-section variation in 260 neutron energy group



shows the cross-section of this reaction in the 260 energy group used by FLUKA [12, 13] Monte Carlo code for low energy neutron transport simulations. The cross-section curve shown in Fig. 1 has been extracted from the JENDL 4.0 library [14] using NJOY2016 [15] nuclear data processing code. The maximum group-averaged cross-section is nearly 10 b. The cross-section corresponding to thermal neutrons is nearly 0.13 b [16]. The resonance integral of the reaction is 6.9 b [17]. Clearly, there exists a possibility to increase the yield of ^{99}Mo through the neutron capture (in ^{98}Mo) route by shifting the photo-neutron spectrum into the epi-cadmium energy region by controlled moderation. If a dominant fraction of neutrons stays in the epi-cadmium region of the spectrum (instead of complete thermalisation to thermal region), the effective cross-section of neutron capture in ^{98}Mo can be more than the cross-section corresponding to thermal neutrons.

An increase in the effective cross-section of $^{98}\text{Mo}(n,\gamma)^{99}\text{Mo}$ reaction due to shifting the neutron spectrum to the epi-cadmium region, has been demonstrated in the IRT-T research reactor, Russia. Here, light water was replaced by beryllium oxide at some irradiation locations inside the reactor core [17]. This resulted in under moderation of neutrons at those locations and consequently, the effective cross-section of $^{98}\text{Mo}(n,\gamma)^{99}\text{Mo}$ reaction was reported to increase up to 0.70 b. Another similar work carried out in the Tehran research reactor (TRR) [18], reported

that the effective cross-section of this reaction could be increased up to 0.52 b.

The present work aims to utilize the under-moderated neutron spectrum obtained from tantalum-beryllium oxide-high density polyethylene (Ta-BeO-HDPE) set-up at an electron accelerator, for ^{99}Mo production. The energy distribution of photo neutrons was shifted from fast to epi-cadmium energy region by moderation (under moderation) using HDPE. The effective cross-section of the reaction was measured using the foil activation method. Thin metal foils of Mo, Au, and Cu were irradiated in the moderated neutron field emerging from the Ta-BeO-HDPE set-up. Høgdahl convention [19] was used for data analysis, to determine thermal and epi-cadmium neutron fluxes.

The following section of this article gives the details of the experiment carried out. The subsequent section describes the theory and the methods used. This is followed by a discussion regarding the data analysis for the experiment. In the subsequent section, results are compared with theoretical simulations and the last section gives the conclusions.

Experimental details

The experiment for the feasibility study of ^{99}Mo production through the (e- γ -n) reaction route was carried out at the 10 MeV electron accelerator at Electron Beam Centre

(EBC), Kharghar, Navi Mumbai, India [20]. The electron accelerator used for the present experiment is a 10 MeV RF industrial electron LINAC having a peak beam current of 0.25 mA. The average output beam power for the accelerator can be varied from 1–3 kW. The accelerated electron beam comes out through a 50 μm thin Ti window and falls vertically down on a 1.8 mm thick Ta sheet. The Ta sheet acts as a photo neutron converter and is placed at a distance of 10 cm from the Ti window. The thickness of the Ta sheet is optimum to produce bremsstrahlung photons by using 10 MeV electrons [11]. The length of the Ta sheet is 1 m and the width of the sheet is 10 cm. There is also a provision for water-based cooling system for Ta foil. Water flows on either side of the central 6 cm region (where the electron beam strikes Ta foil). During the present experiment, the electron beam emerging from the exit window scanned across the 68 cm length of the Ta sheet. This was required to maintain the integrity of the Ti window. The electron beam width along the width of Ta foil was 6 cm.

For the (e- γ -n) reaction experiment at the 10 MeV electron accelerator described above, three cubical shaped beryllium oxide blocks, each having area of 10 cm \times 10 cm

and a thickness of 5 cm placed side by side at a distance of about 2 cm from the Ta converter. This was followed by 3 cm thick HDPE blocks having an area of 10 cm \times 10 cm. The slowing down length of fast neutrons in HDPE is about 5.7 cm [21]. A schematic of this Ta-BeO-HDPE set-up is shown in Fig. 2. The actual image of the experimental set-up is shown in Fig. 3. Bare/cadmium-covered gold (Au) and molybdenum (Mo) foils and a bare copper (Cu) foil was placed on the exit end of central HDPE block. The positions of the installed foils are shown in Fig. 4. For cadmium-covered foils, activation monitors were sandwiched between two cadmium disks. Each of the disks had a thickness of 1 mm.

After installation of the foils on the exit face (the one opposite to the direction of incoming electrons) of the Ta-BeO-HDPE set-up, the accelerator was operated at 3 kW power for nearly 2 h. The foils were retrieved after a cooling period of nearly 30 min. These foils were then counted on a p-type HPGe detector having a relative efficiency of 30%. HPGe detector output was analyzed using an 8 k multichannel analyzer. The energy resolution of the system was 1.8 keV for 1332.5 keV of ^{60}Co .

Fig. 2 Schematic of the Ta-BeO-HDPE setup at the 10 MeV electron accelerator

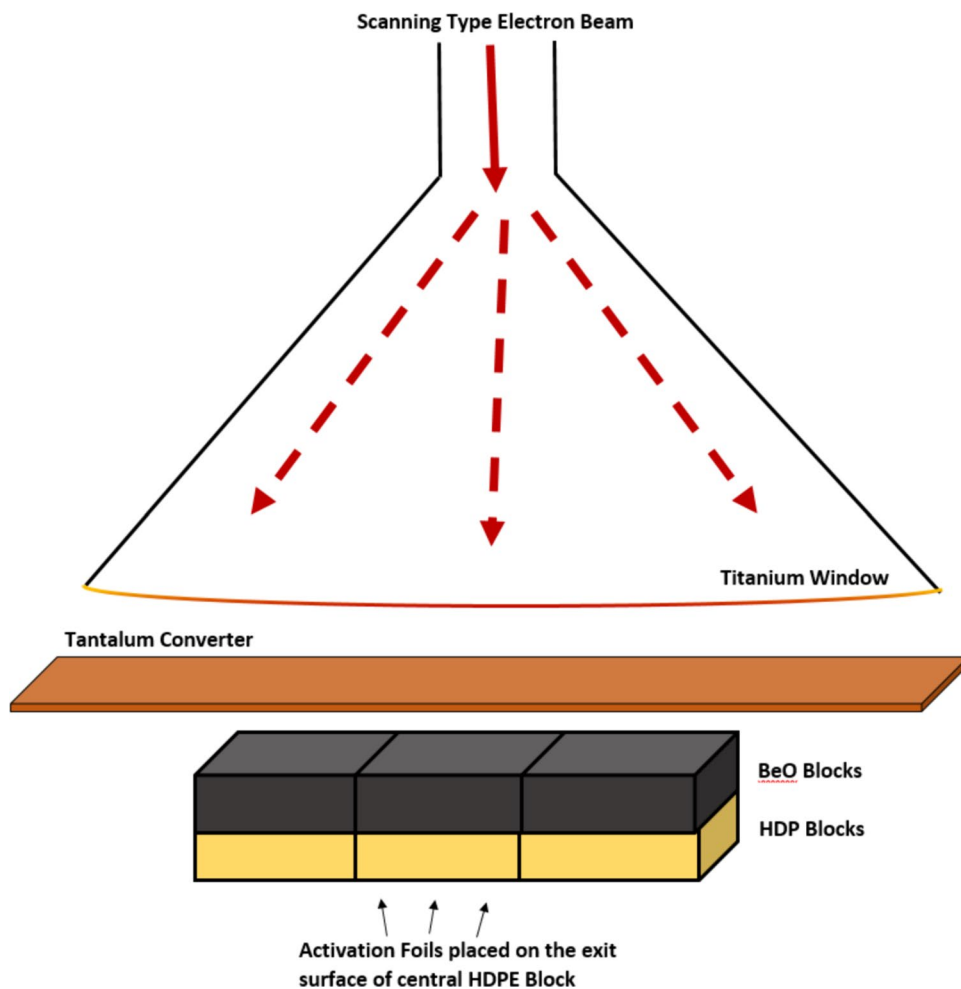


Fig. 3 Actual experimental set-up

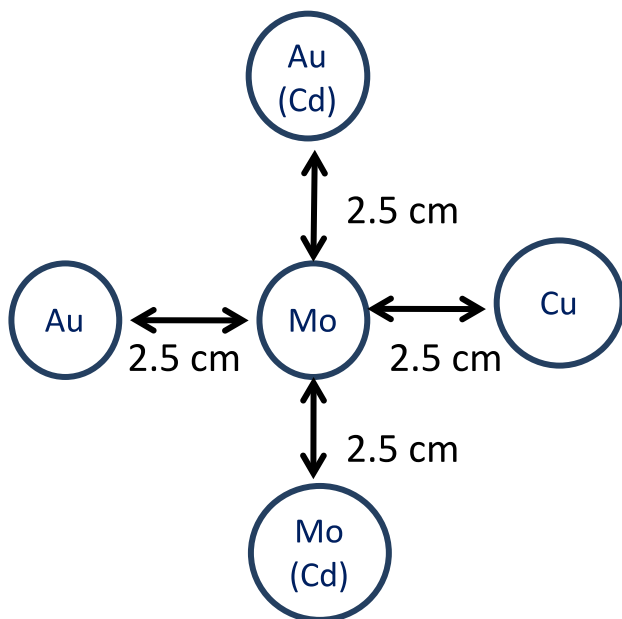
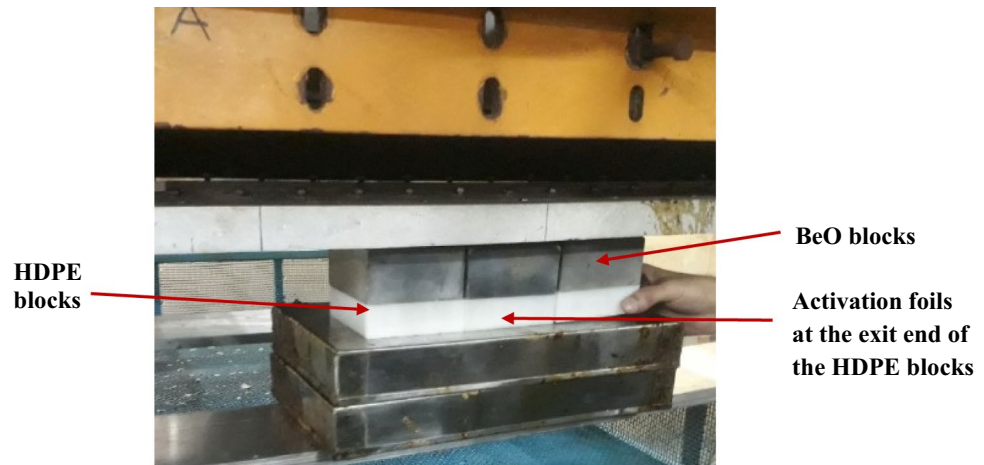


Fig. 4 Placement of the activation foils on the emergent face of the central HDPE block

Standard gamma sources (^{137}Cs (662 keV) and ^{60}Co (1173 keV and 1332 keV)) were used for energy calibration of the spectrometer system used for counting gamma activities. Efficiency calibration was done using a ^{152}Eu standard source having a similar diameter to that of the sample. The measured photo peak efficiencies of prominent and distinct gamma lines were fitted into the following logarithmic empirical function for efficiency calibration.

$$\ln(\varepsilon_\gamma) = \sum_{i=0}^n A_i (\ln(E_\gamma))^i$$

where ε_γ is the full energy peak efficiency at a given gamma energy of E_γ and A_i is regression coefficients obtained from the fitting of measured efficiency data with energy.

The induced gamma activities in the irradiated activation detectors were used to estimate the corresponding microscopic reaction rates (per atom per sec). HØgdahl convention [19] was used to infer the thermal and epi-cadmium neutron fluxes from these reaction rates. The effective cross-section of $^{98}\text{Mo}(n,\gamma)^{99}\text{Mo}$ reaction was obtained from its measured reaction rate and total measured neutron flux at the irradiation location.

Theoretical background of the data analysis

Reaction rate of activation monitor

Induced gamma activity in an irradiated activation foil can be given by the relation [22]:

$$A_n \left(\frac{T_c}{T_i} \right) = N \varepsilon_1 \varepsilon_2 \varepsilon_3 (1 - e^{-\lambda T_i}) e^{-\lambda T_d} G(\tau) F(\tau) \frac{(1 - e^{-\lambda T_c})}{\lambda} \int \sigma_A(E) \phi(E) dE \quad (1)$$

where A_n is the net area of the full energy photo-peak, T_i and T_c are the live time and real time, respectively. N is the number of target atoms, ε_1 is the isotopic abundance of target nuclides, ε_2 is the yield of gamma energy being counted, ε_3 photo-peak efficiency of detector for the gamma energy of interest, λ is the decay constant, T_i , T_d , and T_c are irradiation, cooling and counting times, respectively, $G(\tau)$ is the self-shielding correction factor for the foil, $F(\tau)$ denotes the flux depression factor for the foil, σ_A is the activation cross-section for the reaction of interest at energy E , $\phi(E)$ is the neutron flux at the location of irradiation and τ represents the thickness of the foil.

The saturated reaction rate per atom can be obtained from Eq. (1) as follows:

$$\int \sigma_A(E)\phi(E)dE = \frac{A_n \left(\frac{T_c}{T_i} \right) \lambda}{N \varepsilon_1 \varepsilon_2 \varepsilon_3 (1 - e^{-\lambda T_i}) e^{-\lambda T_d} (1 - e^{-\lambda T_c}) G(\tau) F(\tau)} \quad (2)$$

Estimation of neutron self-shielding factor

The neutron self-shielding correction factor takes care of the attenuation of the flux inside the activation foil due to the absorption of neutrons by the foil material itself. This factor depends on the neutron energy spectrum, geometry, and dimensions of the sample. It is defined as the ratio of the specific activity of the irradiated target to the specific activity of an irradiated infinitely dilute target. The self-shielding correction factor is negligible in the case of an infinite dilution sample.

$$G = \frac{\int_{E_1}^{E_2} \phi^*(E) \sigma_A(E) d(E)}{\int_{E_1}^{E_2} \phi(E) \sigma_A(E) d(E)} \quad (3)$$

where ϕ^* is the perturbed neutron flux inside the sample and ϕ is the neutron flux in the case of an infinite dilution sample. For practical purposes, the integration limits are taken from 0 to 0.5 eV (cadmium cut-off energy) in the case of thermal neutrons and 0.5 eV to 10 MeV in the case of epi-cadmium neutrons.

Analytical formulas are available to calculate the self-shielding factors [23]. However, for calculating self-shielding factors using analytical formulas, various approximations are assumed. These lead to uncertainties in the calculated self-shielding factors. In the present work, thermal and epi-cadmium self-shielding factors of Au, Cu, and Mo foils were estimated using Monte Carlo simulations [24]. The activation foils were modelled with exact dimensions and self-shielding factors were calculated using Eq. (3). The self-shielding correction factors for the foils used in the present experiment are given in Table 1. The measured

saturated reaction rates per atom for the irradiated foils are also given in Table 1.

Measurement of neutron flux

Photo neutrons produced in the Ta converter have a distribution over energy. Determination of neutron flux/spectrum in such cases is often carried out using conventions like Westcott and Høgdahl. The neutron energies are segregated into two groups. Neutrons having energies below 0.5 eV are referred to as thermal neutrons and those having energies above 0.5 eV, are called epi-cadmium neutrons. Westcott convention is used to determine the neutron fluxes and characterize an irradiation location having well-moderated thermal neutron flux (for example, inside a thermal reactor core). This convention was used in flux determination at irradiation location and estimation of $^{98}\text{Mo}(n,\gamma)^{99}\text{Mo}$ effective cross-section in earlier works [17, 18]. However, in the present experiment, neutrons are under-moderated and epi-cadmium flux is quite significant. Westcott convention has a limitation in such cases. Hence, Høgdahl convention has been used in this work.

In a bare, thin activation detector exposed to a thermal/epi-cadmium neutron flux, the reaction rate per atom per sec (RR), according to the Høgdahl convention, is given as follows:

$$\text{RR} = g \sigma_0 G_{\text{th}} \phi_0 + I_0 G_{\text{epi}} \phi_e \quad (4)$$

here RR is the microscopic reaction rate induced in the irradiated activation foil, ϕ_0 is the thermal flux, ϕ_e is epi-cadmium neutron flux parameter, σ_0 is the reaction cross-section for thermal neutrons, g is the Westcott factor and I_0 is the resonance integral. G_{th} and G_{epi} are the self-shielding factors for thermal and epi-cadmium neutrons, respectively. The definitions of reaction rate RR, epi-cadmium neutron energy spectrum $\phi_0(E)$, and resonance integral I_0 are as follows:

$$\text{RR} = \int_{E_0}^{\infty} \sigma(E) \phi(E) dE \quad (5)$$

Table 1 Thermal and epi-cadmium self-shielding factors for different foils

Activation foil and reaction	Mass (gm)	Thickness (mm)	Thermal self shielding factor (G_{th})	Epi-cadmium self-shielding factor (G_{epi})	Saturated reaction rate per atom (Sec^{-1})
$^{98}\text{Mo}(n,\gamma)^{99}\text{Mo}$ (Bare)	0.4225	0.28	0.99	0.89	3.22E – 18
$^{98}\text{Mo}(n,\gamma)^{99}\text{Mo}$ (Cd Covered)	0.4225	0.28	0.99	0.89	2.79E – 18
$^{197}\text{Au}(n,\gamma)^{196}\text{Au}$ (Bare)	0.2591	0.13	0.89	0.22	4.33E – 16
$^{197}\text{Au}(n,\gamma)^{196}\text{Au}$ (Cd Covered)	0.2591	0.13	0.89	0.22	1.84E – 16
$^{63}\text{Cu}(n,\gamma)^{64}\text{Cu}$ (Bare)	0.2766	0.30	0.99	0.78	1.43E – 17

$$I_0 = \int_{E_{cd}}^{\infty} \frac{\sigma(E)}{E} dE \quad (6)$$

$$\infty_0(E) = \varphi_e/E \quad (7)$$

Neutron fluxes were first estimated using Au and Cu reaction rates. In the two group (thermal and epi-cadmium) formalism, the expression for RR for these two foils will yield two linear equations. Thermal flux (φ_0) and epi-cadmium flux parameter (φ_e) can be obtained by solving these two equations. It should be noted here that φ_e is not the epi-cadmium flux, rather it is the epi-cadmium flux parameter. In the epi-cadmium energy region, the neutron energy spectrum is given by Eq. (7) i.e. the spectrum is φ_e times inversely proportional to energy E. The value of epi-cadmium neutron flux ($\text{ncm}^{-2} \text{s}^{-1}$) can be obtained by using the value of φ_e and integrating Eq. (7) between energy limit 0.5 eV to 10 MeV, as shown below.

$$\text{Epi - cadmium neutron flux} = \varphi_e \int_{E_{cd}}^{\infty} \frac{1}{E} dE \quad (8)$$

The neutron flux at the irradiation location was also estimated using the 'cadmium difference method'. To separate the activities due to thermal and epi-cadmium neutrons, bare and cadmium-covered foils were irradiated under identical conditions, and induced gamma activities were measured. The method is based on the fact that cadmium is an effective absorber of neutrons below cadmium cut-off energy, E_{Cd} . The neutrons of energies above E_{Cd} get transmitted through it. The commonly accepted value of E_{Cd} is 0.5 eV. Thermal neutron flux can be obtained by using the reaction rates of bare and cadmium-covered Au foils, using Eq. (9) [18].

$$\varphi_0 = \frac{R}{g \cdot \sigma_0} \frac{CR - 1}{CR} \quad (9)$$

where CR (Cadmium Ratio for Au) is defined as the ratio of the reaction rate of bare Au foil to that of cadmium-covered Au foil. In this work, the measured value of CR for Au is 2.35. Using this value of CR, thermal flux (φ_0) was estimated from Eq. (9). Further, this value of thermal flux was used to estimate the epi-cadmium neutron flux parameter (φ_e) from Eq. (4). Subsequently, epi-cadmium flux was obtained using Eq. (8).

Data analysis

Neutron flux estimation was carried out using the Høgdahl convention as well as the cadmium difference method. For the former method, Au and Cu foil activities were used to obtain a set of two linear equations (Eq. 4). The nuclear data for Au and Cu foils used in both the equations

corresponding to Au and Cu foils are given in Table 2. Using the reaction rates, self-shielding factors (Table 1), and nuclear data (Table 2) for Au and Cu monitors, these equations were solved to get the thermal and epi-cadmium flux values.

The neutron fluxes obtained from both the Høgdahl convention and the cadmium difference method are listed in Table 3. It can be seen that the values of total neutron fluxes obtained by both methods are very close to each other, differing by only 2%. The average value of total neutron flux can be taken as $9.51\text{E}+6 \text{ ncm}^{-2} \text{ s}^{-1}$. It can also be seen from Table 3 that the ratio of epi-cadmium to thermal flux is about 2.5, which shows the dominance of epi-cadmium flux.

As, the second step of data analysis, the effective cross-section of $^{98}\text{Mo}(n,\gamma)^{99}\text{Mo}$ reaction was estimated. Figure 5 shows the prominent energy lines observed in the HPG detector for irradiated bare Mo foil. The 740 keV energy peak (having a branching ratio of 12.3%) was used for estimating the reaction rate for $^{98}\text{Mo}(n,\gamma)^{99}\text{Mo}$ reaction. The measured reaction rate was $3.22\text{E}-18 \text{ s}^{-1}$. This reaction rate was for a finite thickness of Mo foil. Hence, it had to be corrected for the self-shielding effect (Table 1). Effective cross-section for $^{98}\text{Mo}(n,\gamma)^{99}\text{Mo}$ reaction, is simply, the self-shielding corrected reaction rate divided by the total neutron flux. The effective cross-section of $^{98}\text{Mo}(n,\gamma)^{99}\text{Mo}$ reaction was found to be 0.39 b.

Error analysis

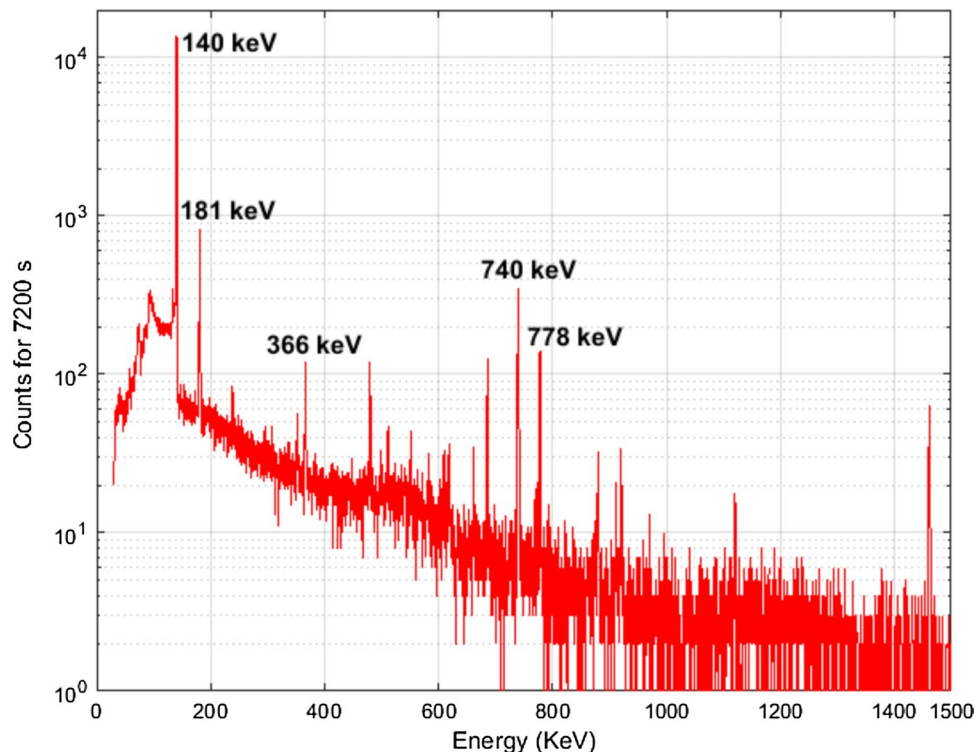
The main components of error in reaction rate, which is the basic measured quantity, are statistical errors in gamma count rates and uncertainty in detector efficiency. The statistical errors in counts corresponding to Au and Cu foils were 0.3% and 0.5%, respectively. In the case of counts for Mo foil, the error was ~2.36%. The reason for a relatively higher value of error was the low count rate in irradiated Mo foil. The uncertainty in detector efficiency was ~2.3%. Hence, the error in Au and Cu reaction rates are 2.32% and 2.35%, respectively. The error in the Mo reaction rate is 3.30%. The uncertainty in the self-shielding factor is less than 0.5%, hence the error in total neutron flux, inferred from the Au and Cu reaction rates is 3.45%. Finally, the overall uncertainty in the effective cross-section comes out to be 4.77%.

Table 2 Nuclear data for Au and Cu foils

Activation foil and reaction	Cross-section, σ_0 (b)	g	I_0 (b)
$^{197}\text{Au}(n,\gamma)^{198}\text{Au}$	98.8	1.005	1550
$^{63}\text{Cu}(n,\gamma)^{64}\text{Cu}$	4.51	1.00	4.9

Table 3 Neutron fluxes at the irradiation location

Flux determination method	Thermal flux (ncm ⁻² s ⁻¹)	Epi-cadmium flux parameter	Epi-cadmium flux (ncm ⁻² s ⁻¹)	Total neutron flux (ncm ⁻² s ⁻¹)
Bare Au and Cu foils	2.71E+06	5.66E+05	6.90E+06	9.61E+6
Bare and Cd covered Au foils	2.83E+06	5.39E+05	6.58E+06	9.41E+6

Fig. 5 Gamma lines observed in HPGe detector for irradiated bare Mo foil

Discussions and comparison with simulations

At the irradiation location in the Ta-BeO-HDPE experimental setup, thermal and epi-cadmium neutron fluxes were measured using two different approaches. It can be seen from Table 3 that the neutron flux values obtained by the two methods are very close to each other. The ratio of epi-cadmium to thermal flux is about 2.55, it shows the dominance of epi-cadmium neutron flux, which is useful for utilizing the resonances for $^{98}\text{Mo}(n,\gamma)^{99}\text{Mo}$ reaction cross-section in the intermediate region. The effective cross-section of $^{98}\text{Mo}(n,\gamma)^{99}\text{Mo}$ reaction in this neutron field is 0.39 ± 0.014 b, which is 3 times the cross-section (0.13b) corresponding to thermal neutrons. The measured cadmium ratio of $^{98}\text{Mo}(n,\gamma)^{99}\text{Mo}$ reaction is 1.23. The inverse of the cadmium ratio is the measure of the relative contribution of epi-cadmium neutrons in the reaction, which is about 81% in this case. This again confirms the dominance of epi-cadmium neutrons contribution in $^{98}\text{Mo}(n,\gamma)^{99}\text{Mo}$ reaction rate.

Simulations

The experimental measurements were compared with the results obtained from Monte Carlo simulations of the set-up. The particle transport code, FLUKA was used to simulate the photon and neutron production/transport across the experimental set-up. FLUKA is a general purpose Monte Carlo code that can handle a wide variety of particles over a wide energy range [25]. Low-energy neutrons are simulated using multi-group formalism. FLUKA has its own 260 energy group library for the same. It can very accurately transport electrons and photons from 1PeV to KeV region. Also, the neutronic interactions are fully coupled to the electromagnetic cascades. FLUKA code was found to be suitable to simulate the (e- γ -n) cascade reactions occurring in the Ta-BeO-HDPE set-up.

A cross-section of the simulated set-up in the Y-Z plane (as implemented in FLUKA) is shown in Fig. 6. The accelerated electrons (emerging from the Ti window) were assumed to incident on a Ta target, along the positive Z-axis. The emitted bremsstrahlung spectrum produced from the

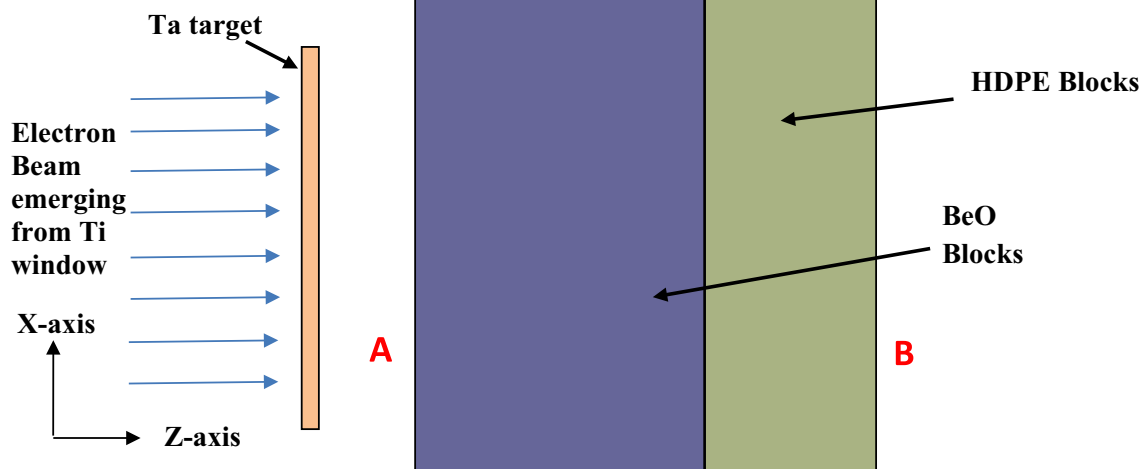


Fig. 6 Cross-section of the Ta-BeO-HDPE set-up (As modelled in FLUKA code)

interaction of 10 MeV electrons in the Ta foil (and incident on BeO blocks) was scored at a distance of 6 mm from Ta foil. The intermediate distance was occupied by an aluminium sheet (6 mm thick), which was meant to provide support to the Ta sheet. The photon spectrum due to electron interactions in Ta foil is shown in Fig. 7. The neutron spectrum was scored at two locations (shown as A and B in Fig. 6) and was averaged over the cross-section of the central BeO/HDPE block. The simulated neutron energy spectra at the two locations are shown in Fig. 8. It can be seen that the neutron spectrum at the exit end of BeO-HDPE blocks

(location B) has an enhanced epi-cadmium component. The neutron spectrum just before the BeO edge, facing the Ta foil is predominantly fast. All the simulation results mentioned in this section correspond to the FLUKA simulations corresponding to 5 cycles with $2.0E+6$ million particle histories in each cycle.

The neutron fluxes and cadmium ratios for Au/Mo foils obtained from the simulated neutron spectrum and those obtained from measurements are compared in Table 4. The cross-sections needed for the estimation of cadmium ratios were obtained from the JENDL 4.0 library [10]. It can be

Fig. 7 Photon spectrum incident on the BeO blocks

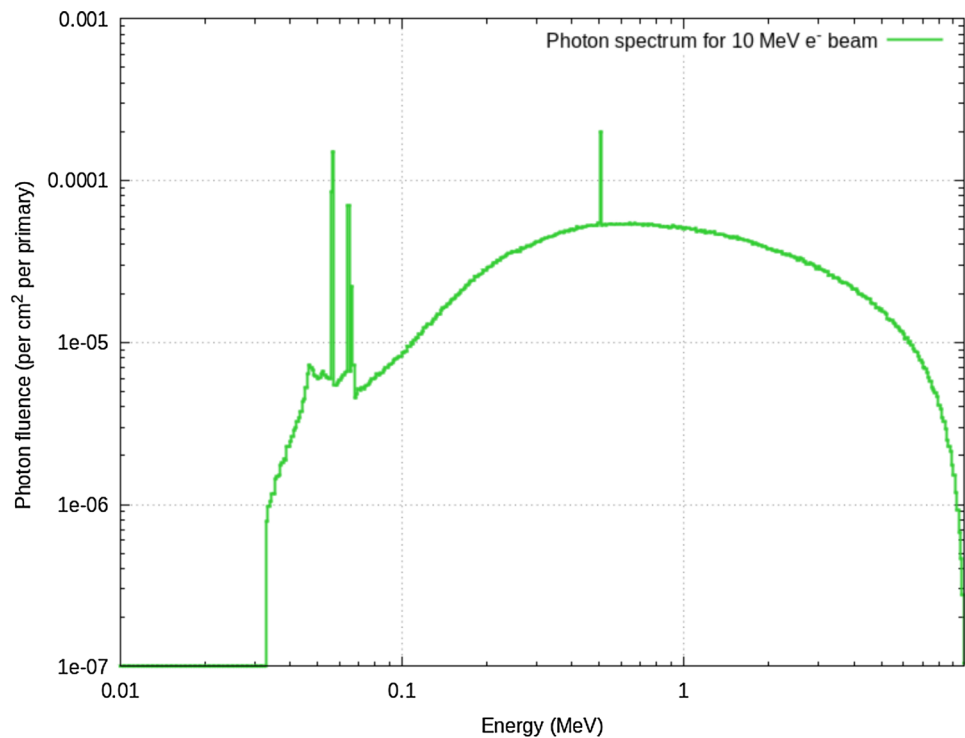
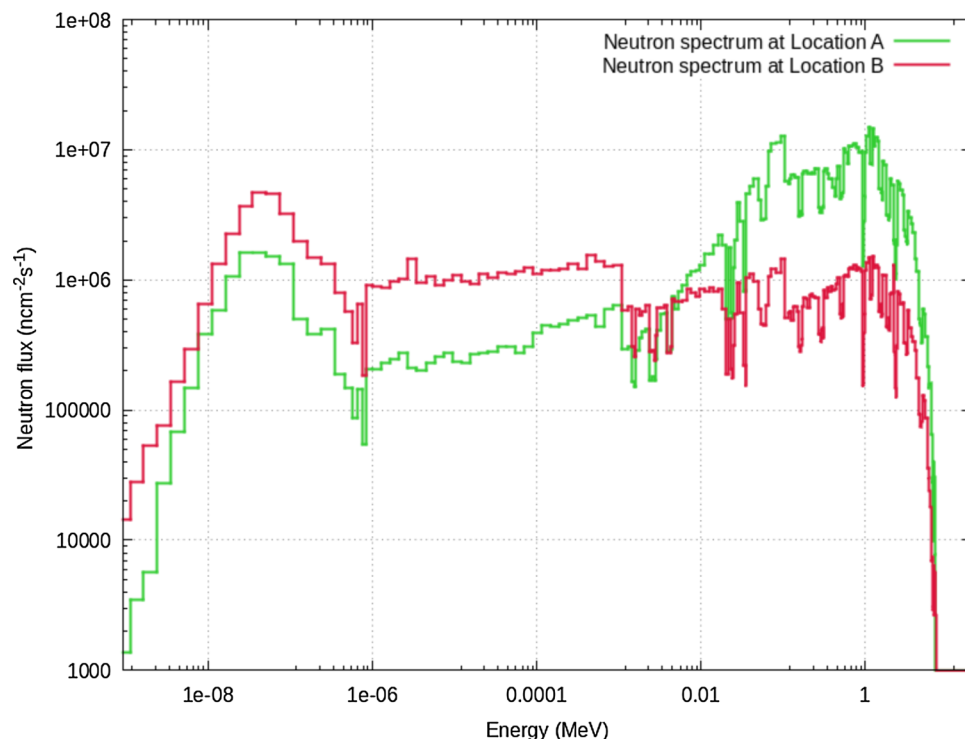


Fig. 8 Neutron spectrum on the incident and the exit face of the BeO-HDPE blocks**Table 4** Neutron fluxes and cadmium ratios at the exit end of the central HDPE block

Flux determination method	Thermal flux (ncm ⁻² s ⁻¹)	Epi-cadmium flux (ncm ⁻² s ⁻¹)	Total neutron flux (ncm ⁻² s ⁻¹)	Red for Au	Red for Mo
Measured Values	2.71E+6	6.90E+06	9.61E+6	2.35	1.23
Values from simulations	2.66E+7	1.32E+08	1.59E+8	2.23	1.07
Values from simulations after applying correction for electron beam scanning	3.91E+6	1.94E+7	2.33E+7	2.23	1.07

seen from Table 4 that the neutron fluxes obtained from the FLUKA simulation of the set-up are higher than the corresponding measured values. The reason for this is the spatial scanning of the electron beam incident on the Ta foil. The average electron beam current during the experiment was 200 μA . The simulated results given in Table 4 correspond to this same value of current. However, since the electron beam scans over a length of 68 cm of Ta foil (along the y-axis), the effective electron current needs to be reduced.

To highlight this fact, in the FLUKA simulations, the electron beam was first assumed to be incident at the center of the Ta foil. The width of the beam in the y-direction was kept at 1 mm. Figure 9 shows the photon fluence distribution in the Y–Z plane, for this case. It can be seen that the bremsstrahlung photons are mostly peaked along the forward direction. The photon fluence distribution in the X–Y plane is shown in Fig. 10. The neutron production in BeO due to these photons will vary with the position of the electron

beam on the Ta foil. Figure 11 shows the neutron fluence distribution (in the X–Z plane) for this case.

The electron beam was then made to fall at $y = 15$ cm (near the top edge of the BeO-HDPE blocks). The photon and neutron fluence distributions (in the X–Y plane) for this case are shown in Figs. 12 and 13. There is a clear reduction in contribution to the neutron flux in the scoring region. To further highlight this effect, a simulation was also carried out with the electron beam hitting the top edge (along the y-axis) of Ta foil ($y = 34$ cm). The photon and resulting neutron fluence distribution in the Y–Z plane for this case is shown in Figs. 14 and 15.

From the results discussed above, it is obvious that both the flux and the spectrum of neutrons at the exit end of HDPE are dependent on the point of interaction of electrons with Ta foil. As the photons and the neutrons generated due to electron beam interaction at different points of Ta foil will travel different distances in BeO and HDPE, this will also affect the corresponding spectrum of neutrons reaching the exit side of

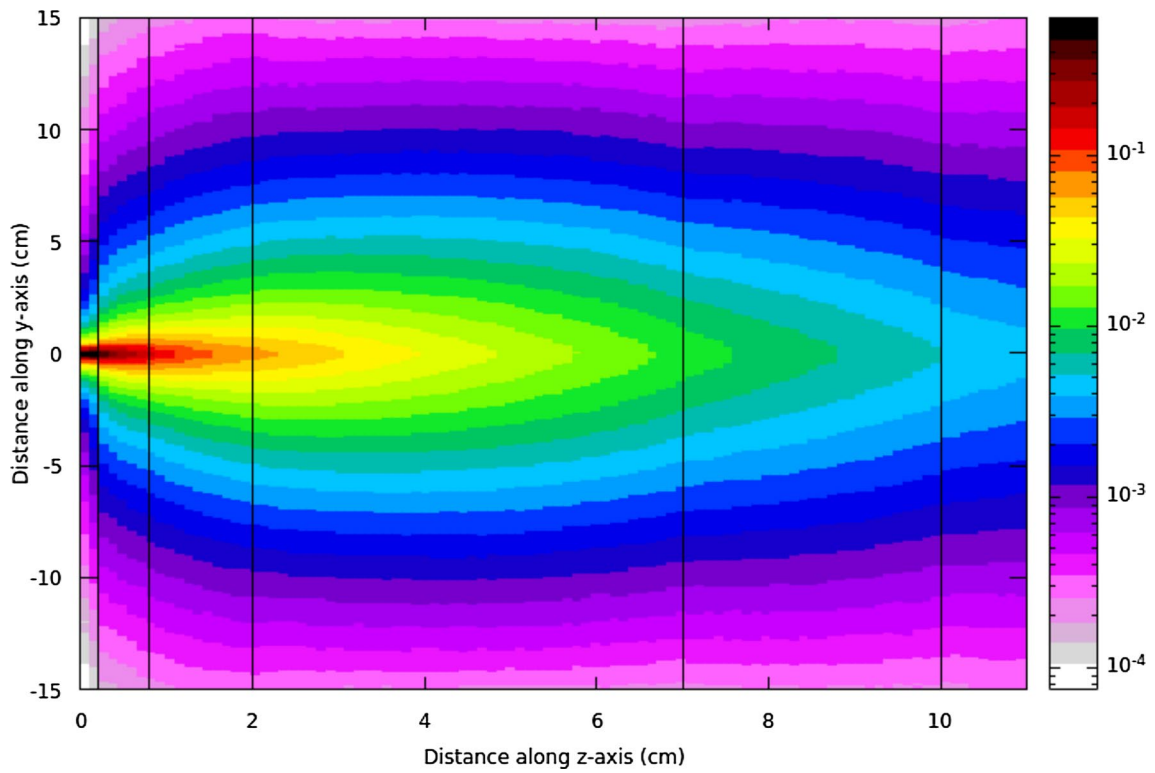


Fig. 9 Photon fluence ($\text{cm}^{-2}\text{primary}^{-1}$) distribution in the Y-Z plane for e^- beam at $y=0$ cm

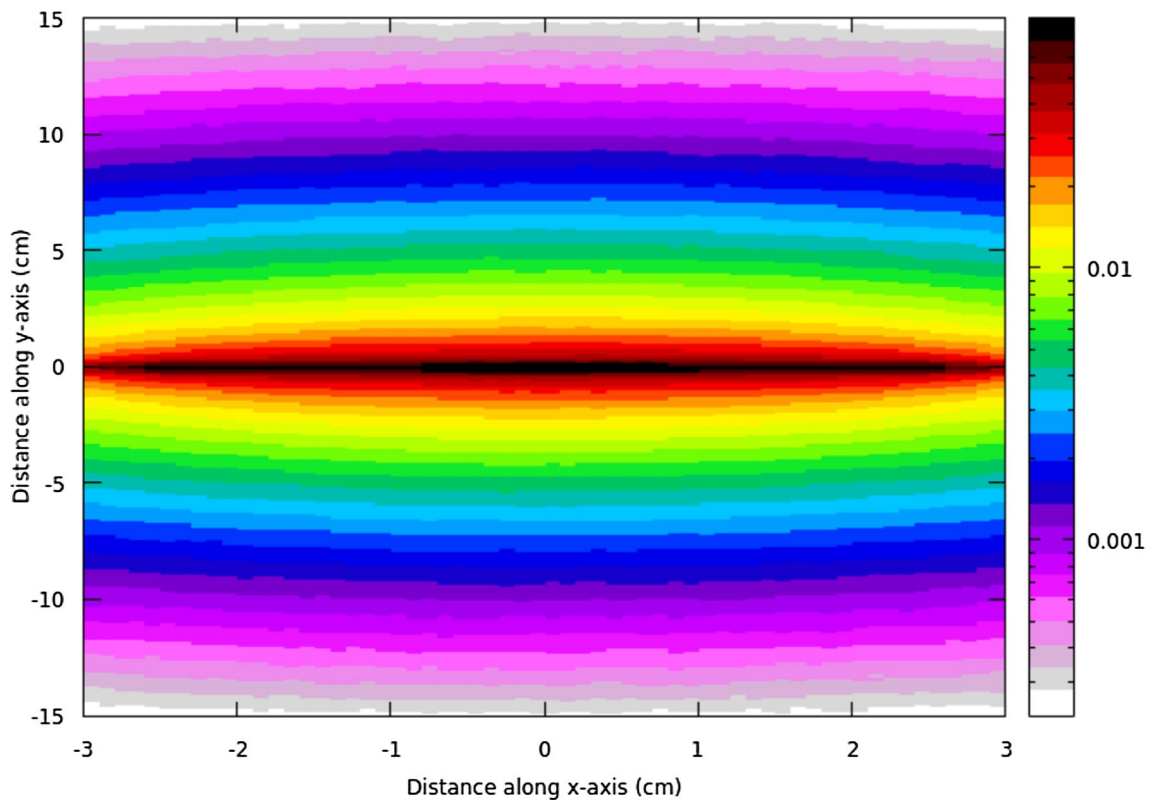


Fig. 10 Photon fluence ($\text{cm}^{-2}\text{primary}^{-1}$) distribution in the X-Y plane for e^- beam at $y=0$ cm

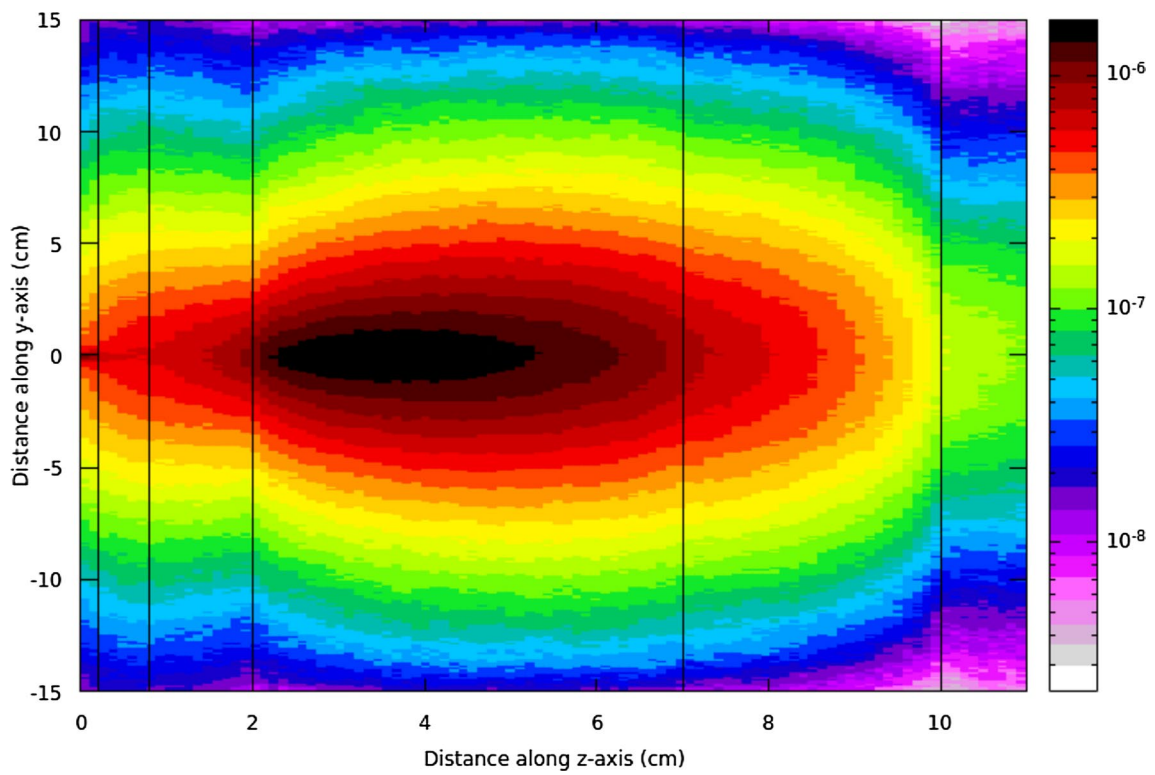


Fig. 11 Neutron fluence ($\text{cm}^{-2}\text{primary}^{-1}$) distribution in the X-Z plane for e^- beam at $y=0$ cm

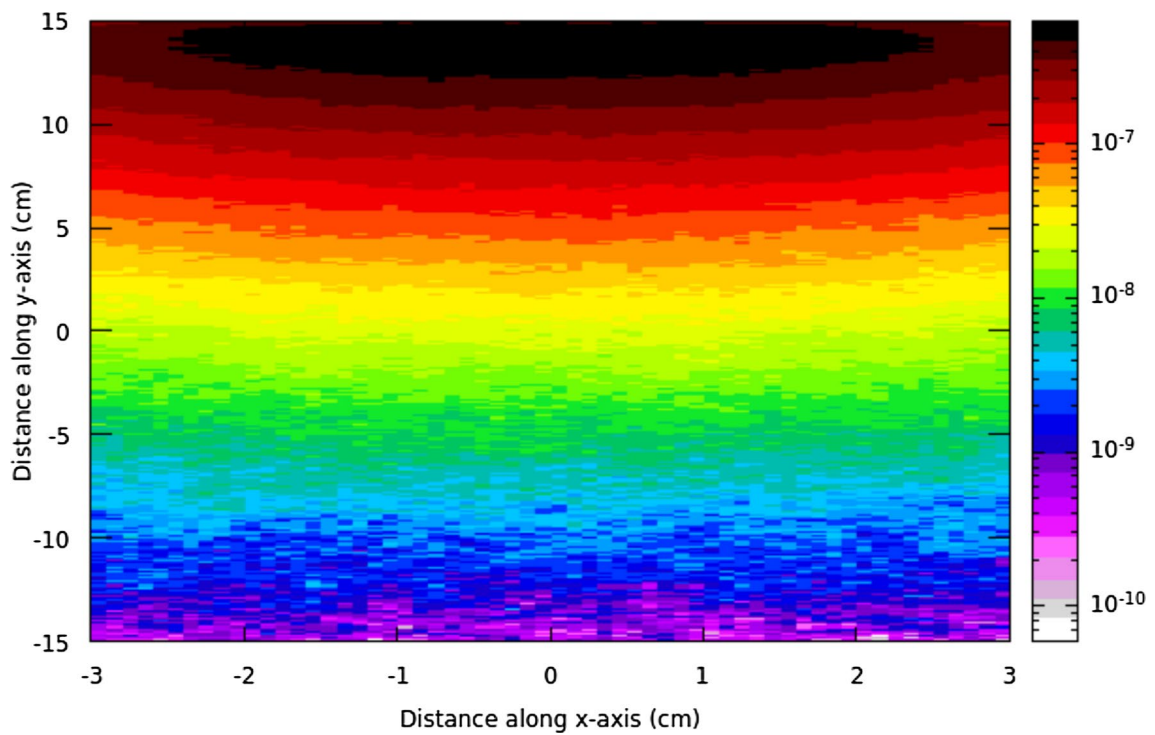


Fig. 12 Photon fluence ($\text{cm}^{-2}\text{primary}^{-1}$) distribution in the X-Y plane for e^- beam at $y=15$ cm

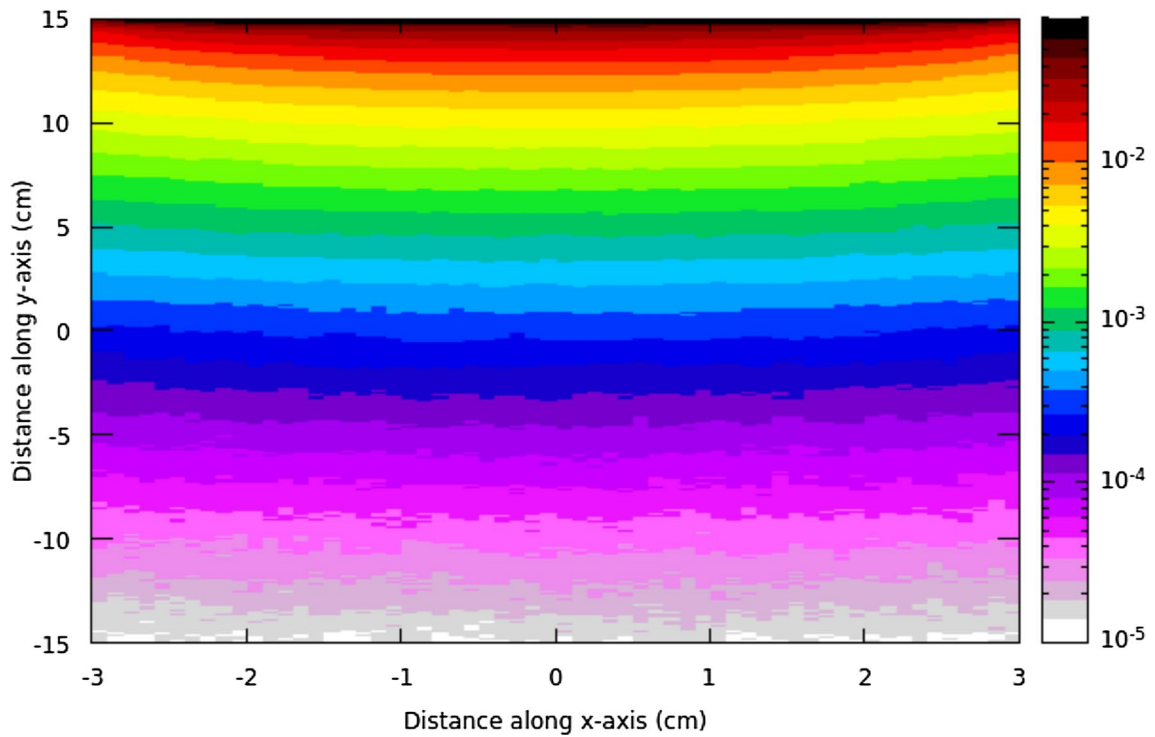


Fig. 13 Neutron fluence ($\text{cm}^{-2}\text{primary}^{-1}$) distribution in the X-Y plane for e^- beam at $y = 15$ cm

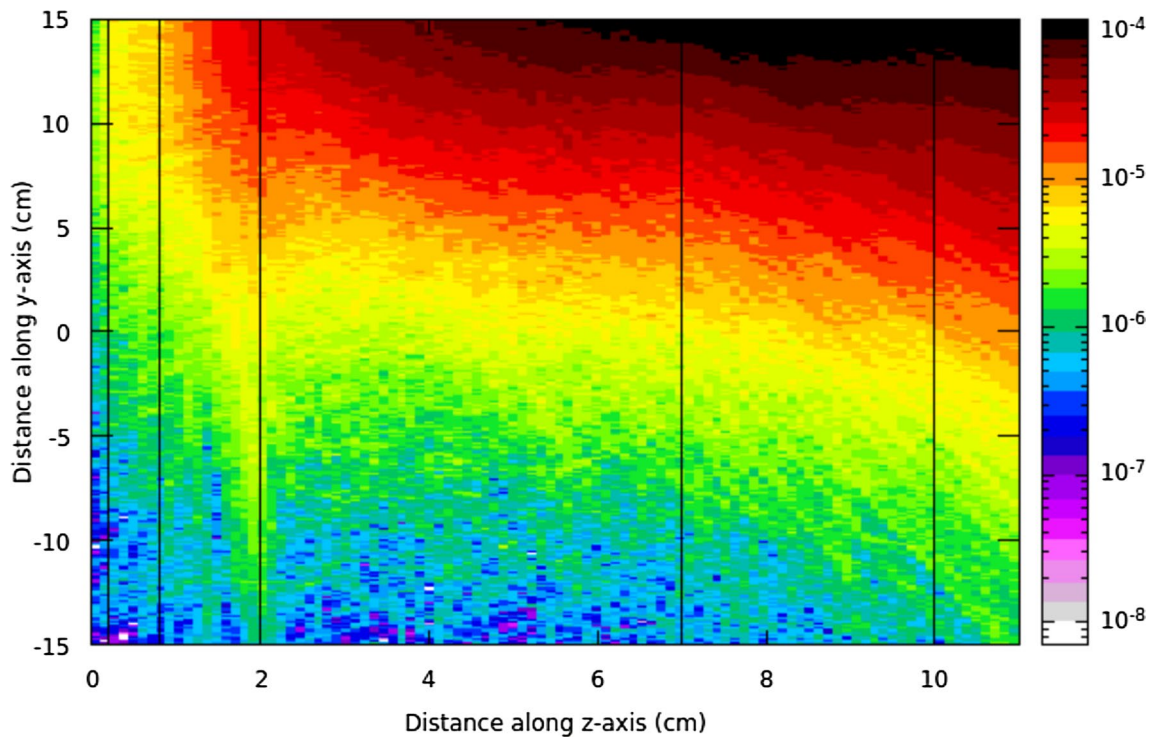


Fig. 14 Photon fluence ($\text{cm}^{-2}\text{primary}^{-1}$) distribution in the X-Y plane for e^- beam at $y = 34$ cm

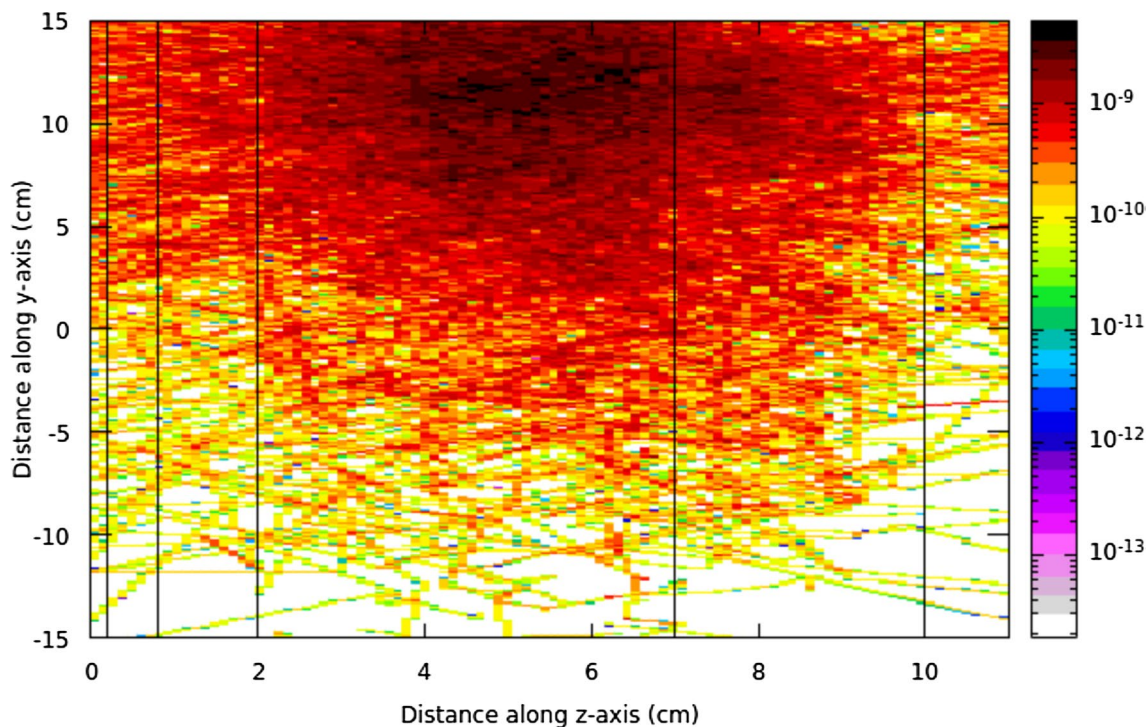


Fig. 15 Neutron fluence ($\text{cm}^{-2}\text{primary}^{-1}$) distribution in the Y–Z plane for e^{-} beam at $y = 34$ cm

HDPE (Location B in Fig. 6). For qualitative analysis, it can be deduced from the fluence distributions, shown in Figs. 9, 10, 11, 12, 13, 14 and 15, that the gammas are mostly concentrated within a distance of 5 cm (along the y-axis) on either side of the point of interaction of electrons with Ta foil. The spread of neutron fluence is larger. However, it may be safe to assume that the electrons falling within the line of sight of a particular HDPE block will have a maximum contribution to the neutron flux at the exit end of the block.

The effective electron current and the subsequent flux were reduced by a fraction equal to the ratio of the width of the central BeO-HDPE block (10 cm) and the distance over which the electron beam scans (68 cm). The values of fluxes obtained at the exit end of the central HDPE block was normalized with this factor, which comes out, be 0.15 (see Table 4). There is a good agreement of the normalized values with the measured values. The small difference in the measured and simulated cadmium ratio values for Au and Mo can be attributed to the difference in the spectrum of neutrons corresponding to different points of interaction of the electron beam with the Ta converter.

Conclusion

Effective cross-section of $^{98}\text{Mo}(n,\gamma)^{99}\text{Mo}$ reaction was measured in an electron accelerator driven photo-neutron source, having epi-cadmium dominant neutron energy

spectrum. Enhancement of $^{98}\text{Mo}(n,\gamma)^{99}\text{Mo}$ reaction cross-section by three times compared to the corresponding value in the thermal neutron spectrum was demonstrated experimentally. The increment in the effective cross-section can be attributed to the presence of large resonances of ^{98}Mo in the epi-cadmium region of the neutron spectrum. The enhancement in effective cross-section has a direct significance in increasing ^{99}Mo yield through the neutron capture route in ^{98}Mo .

A good agreement between the measurements and Monte Carlo simulations of the present Ta-BeO-HDPE configuration, using FLUKA code was encouraging. The theoretical simulations will be used for the optimization of the set-up and planning future experiments in this regard. The final aim is to explore the feasibility of ^{99}Mo production using electron accelerators. Although the neutron flux in the present work was low ($9.51\text{E}+6 \text{ ncm}^{-2} \text{ s}^{-1}$), the results indicate that a high current and high energy electron accelerator can emerge as an alternative to nuclear reactor for ^{99}Mo production using neutron capture in ^{98}Mo .

Acknowledgements We are thankful to Dr. Tushar Roy and Dr. Yogesh Kashyap, TPD, BARC for their help regarding the experimental set-up. Our thanks are due to Dr. S. V. Thakare, RPhD in the initial discussion pertaining to this work. Discussion about self-shielding estimation with Shri Anek Kumar and Shri Devesh Raj, RPDD was very useful.

Funding Open access funding provided by Department of Atomic Energy.

Declarations

Conflict of interest The authors declare that they have no conflict of interests/competing interests that are directly or indirectly related to the work submitted for publication.

Open Access This article is licensed under a Creative Commons Attribution 4.0 International License, which permits use, sharing, adaptation, distribution and reproduction in any medium or format, as long as you give appropriate credit to the original author(s) and the source, provide a link to the Creative Commons licence, and indicate if changes were made. The images or other third party material in this article are included in the article's Creative Commons licence, unless indicated otherwise in a credit line to the material. If material is not included in the article's Creative Commons licence and your intended use is not permitted by statutory regulation or exceeds the permitted use, you will need to obtain permission directly from the copyright holder. To view a copy of this licence, visit <http://creativecommons.org/licenses/by/4.0/>.

References

1. The supply of medical radio isotopes (2010): Review of potential Mo-99/Tc-99 production technology: A report by nuclear energy agency, OECD
2. IAEA Research Reactor Database <https://www.iaea.org/resources/databases/research-reactor-database-rrdb>. Accessed 19 October 2023
3. Valeriia N et al (2014) Production of medical radioisotopes with linear accelerators. *Appl Radiat Isot* 85:39–44
4. Gopalakrishna A, Naik H, Suryanarayana SV, Naik Y, Nimje VT, Nayak BK, Sarkar SK, Padmanabhan S, Kothalkar C, Naskar P, Dey AC, Goswami A (2016) *J Radioanal Nucl Chem* 308(2):431–438
5. Naik H, Kim GN, Kapote Noy R, Schwengner R, Kim K, Zaman M, Shin SG, GeyMassarczyk YR, John R, Junghans A, Wagner A, Cho M-H (2016) *Eur Phys J* 52:195
6. Naik H et al (2013) An alternate route for Mo-99 production from U-238(γ , f) and Mo-100 (γ , f) reaction. *J Radioanal Nucl Chem* 295:807–816
7. Crasta R et al (2011) Measurement of Photo neutron cross-section of 100-Mo (γ , n). *J Radioanal Nucl Chem* 295:367–373
8. Gopalakrishna A, Kim GN, Naik H, Kim K, Nayak BK, Zaman M (2018) *J Radioanal Nucl Chem* 316:561–569
9. Parashari S, Mukherjee S, Suryanarayana SV, Nayak BK, Makwana R, Singh NL, Naik H (2019) *Phys Rev C* 99:044602
10. Capogni M et al (2018) ^{99m}Tc by ^{99}Mo produced at the ENEA-FNG facility of 14 MeV neutrons. *Appl Radiat Isot* 134:105–107
11. Eshwarappa KM et al (2005) Estimation of photo neutron yield from Beryllium target in Microtron. *Nucl Instrum Methods Phys Res A* 540:412–418
12. Bohlen TT et al (2014) The FLUKA Code: Developments and challenges for high energy and medical applications. *Nucl Data Sheets* 120:211–214
13. Ferrari A et al (2005) FLUKA: a multi-particle transport code. CERN-2005–10, INFN/TC_05/11, SLAC-R-773
14. Shibata K et al (2011) JENDL-4.0: a new library for nuclear science and engineering. *J Nucl Sci Technol* 48(1):1–30
15. Macfarlane R et al (2016) The NJOY nuclear data processing system, Version 2016 LA-UR-17–20093
16. Badwar S et al (2017) Measurement of formation cross-section of ^{99}Mo from the ^{98}Mo (n, γ) and ^{100}Mo (n,2n) reactions. *Appl Radiat Isot* 129:117–123
17. Ryabchikov AI et al (2004) Obtaining molybdenum-99 in the IRT-T research reactor using resonance neutrons. *Nucl Instrum Methods Phys Res B* 213:364–368
18. Jokar AR et al (2014) Measurement of effective neutron cross-section of the reaction ^{98}Mo (n, γ) ^{99}Mo in TRR nuclear reactor by using thermal neutrons. *Ann Nucl Energy* 63:653–657
19. ASTM report (2021) Standard practice for determining neutron fluence, fluence rate, and spectra by radioactivation techniques. In: ASTM International, Designation: E261–16
20. <https://www.barc.gov.in/technologies/linac/index.html>. Accessed 16th May 2023
21. Glasstone and Edlund (1952) *Element of nuclear reactor theory*. D VanNostrad Company, New York
22. Naik H, Suryanarayana SV, Mulik VK et al (2012) Measurement of the neutron capture cross-section of ^{238}U using the neutron activation technique. *J Radioanal Nucl Chem* 293:469–478
23. Martinho E et al (2003) Universal curve of epithermal neutron resonance self-shielding factors in foils, wires and spheres. *Appl Radiat Isot* 58:371–375
24. Bhandari D et al (2021) Determination of spectrum shaping factor in nuclear reactor AHWR-CF by Monte Carlo method for material characterization using neutrons. *Mater Today: Proc* 38(Part 5):3041–3045
25. Battistoni G (2015) Overview of the FLUKA code. *Ann Nucl Energy* 82:10–18

Publisher's Note Springer Nature remains neutral with regard to jurisdictional claims in published maps and institutional affiliations.